An attention-based deep-learning system with fMRI functional connectivity optimized frequency EEG microstates classifies distinct temporal cortical communications of different cognitive tasks

Swati Agrawal
NMR Research Centre Institute of Nuclear Medicine and Allied Sciences (INMAS)
Vijayakumar Chinnadurai (vijayakumar.inmas@gov.in)
NMR Research Centre Institute of Nuclear Medicine and Allied Sciences (INMAS)
Rinku Sharma
Delhi Technological University

Research Article

Keywords: Attention-based deep learning, Frequency-microstates, Hemodynamic functional connectivity, EEG informed fMRI. Multifrequency coupling, Target detection

Posted Date: April 15th, 2022

DOI: https://doi.org/10.21203/rs.3.rs-1550374/v1

Abstract

Temporal analysis of global cortical communication of cognitive tasks in coarse EEG information is still challenging due to the underlying complex neural mechanisms. This study proposes an attention-based time-series deep learning framework that processes fMRI functional connectivity optimized quasi-stable frequency microstates for classifying distinct temporal cortical communications of the cognitive task. Seventy volunteers were subjected to visual target detection tasks, and their electroencephalogram (EEG) and functional MRI (fMRI) were acquired simultaneously. At first, the acquired EEG information was preprocessed, and the band passed to delta, theta, alpha, beta, gamma bands and then subjected to quasi-stable frequency-microstate estimation. Subsequently, time-series elicitation of each frequency microstates is optimized with graph theory measures of simultaneously eliciting fMRI functional connectivity between frontal, parietal, and temporal cortices. The distinct neural mechanisms associated with each optimized frequency-microstate were analyzed using microstate-informed fMRI. Finally, these optimized, quasi-stable frequency microstates were employed to train and validate the attention-based Long Short-Term Memory (LSTM) time-series architecture for classifying distinct temporal cortical communications of the target from other cognitive tasks. Based on the stability of transition probabilities of the optimized microstates, three different temporal sampling windows (200, 300, and 500 ms/segment) have been employed to collect the input microstates information for these time-series deep-learning systems. Our results revealed twelve distinct frequency microstates capable of deciphering target detections' temporal cortical communications from other task engagements. Particularly, fMRI functional connectivity measures of target engagement were observed significantly correlated with the right-diagonal delta (r=0.31), anterior-posterior theta (r=0.35), left-right theta (r=-0.32), alpha (r=-0.31) microstates. Further, neuro-vascular information of microstate-informed fMRI analysis revealed the association of delta/theta and alpha/beta microstates with cortical communications and local neural processing, respectively. The classification accuracies of the attention-based LSTM were higher than the traditional LSTM architectures. Particularly, the attention-based LSTM sampled microstates for 300 ms revealed a higher classification accuracy of 96% compared with other attention-based LSTM models with 200 ms (95%) and 500 ms (93%) temporal sampling windows. In conclusion, the study demonstrates reliable temporal classifications of global cortical communication of distinct tasks using an attention-based deep learning framework utilizing fMRI functional connectivity optimized quasi-stable frequency microstates.

1. Introduction

1.1 Decoding distant cortical communications from cortical EEG

The human brain dynamically engages distinct neural populations between distant brain regions, and their spatiotemporal oscillations often modulate systematically with behavioural and cognitive tasks. Many distantly located local brain circuitry performs specific localized jobs during such a neural

engagement. The synchrony or lack thereof between these remote brain regions brings effective global brain communication for information processing and is measured as functional connectivity dynamics in acquired task functional MRI and cortical EEG information. Many researchers (Kiehl and Liddle 2003; Laufs et al. 2003; Mantini 2007) employed simultaneous EEG information acquired with fMRI imaging to understand these functional connectivities, neural origins, and correlated brain states. These researches revealed that the elicitation of local neural systems is observed as high-frequency dynamics in EEG cortical oscillations. Cortical high-frequency gamma oscillation mainly explains local high-level neural information and positively correlates with the fMRI BOLD strength. The distant cortical and long-range coordination emerges as the lower EEG cortical frequency oscillation (Buzsáki 2009). The alpha and beta power modulate the BOLD response's latency and strength to gamma power changes (Magri et al. 2012). However, many researchers (Murta et al. 2017) subsequently observed that multi-frequency cortical EEG interaction explains hemodynamic task elicitation better than single EEG power information. JC Pang et al (Pang and Robinson 2018) revealed that the inverse correlation of alpha and BOLD originates from high- and low-frequency components of the same underlying neural engagement caused by modulation in corticothalamic and intra-thalamic feedback. Despite these clear insights of distinct global and local neural processing associated with every task engagement, decoding their temporal dynamics computationally from spatially coarse-grained cortical times-series EEG information is still a challenge.

1.2 Microstates and global cortical communication

Microstates are the cluster centers unique in every cognitive task engagement in healthy and disease populations. Every microstate topography is associated with a "quasi-stable" functional state (Gschwind et al. 2016; Michel and Koenig 2018), explaining the brain's specific neural interaction. These quasi-stable patterns span around 100 ms are the most robust approach to bringing distant functional communication in cortical EEG information. Many researchers (Yuan et al. 2012; Khanna et al. 2015) observed that the time course of microstate metrics when correlated with the fMRI BOLD signal, reveals functional networks similar to the resting-state networks. Further, the microstate dynamics are observed to measure transitions between global cortical communications characterized by specific local neural alpha inhibitions (Milz et al. 2017; Croce et al. 2020; Kaur et al. 2020; von Wegner et al. 2021). The microstate estimation inherently employs the EEG frequency range (Koenig et al. 2002; Pascual-Marqui et al. 2014) of 2-20Hz, making their time-series dynamics explain the cortical alpha inhibitory/excitatory modulations (Milz et al. 2016). However, the cognitive task engagement's distant and local cortical communication manifests through other EEG rhythms (Hipp et al. 2011; Ribary et al. 2017). Thus, the task-induced modulation of cortical communication and associated local neural engagement are manifested as a combination of different frequencies (Akam and Kullmann 2014). More recently, the beta-band and the coverage feature of the EEG microstate analysis have been revealed as the essential features for the classification of epilepsy and PNES patients with reasonably high accuracy and precision (Ahmadi et al. 2020).

1.3 Deep learning approaches for time-series EEG analysis

The EEG time-series information is higher-dimensional data, and the cognitive information is spread across its timelines. Hence, the feature information derived from a single time point of EEG time series data is inadequate to explain any cognitive process. Thus, Recurrent Neural networks (RNN) perform better in extracting sequential information embedded in higher dimensional EEG time-series information. However, the traditional RNN system suffers in learning long-term dynamics due to vanishing/exploding gradient problems. Long Short-Term Memory (LSTM) architecture addresses this exploding gradient obstacle by learning both long- and short-term dependencies. Recently, the attention mechanism has been introduced (Vaswani, A. 2017) to improve the performance of deep learning models; it highlights the more informative feature and subsequently gives higher weights to the corresponding original feature sequence. It has been embedded with the LSTM architecture in several EEG studies (Zhang et al. 2018, 2020b; Karim et al. 2019; Xie et al. 2019; Yan et al. 2019; Jin et al. 2020; Kim and Choi 2020; Rashid et al. 2020; Yao et al. 2020; Jiang et al. 2021; Zheng and Chen 2021) by effectively selecting the feature information and observed with significantly improved efficiency and performance accuracy of deep learning systems.

1.4 Present Study

The present study proposes an attention-based LSTM computational model that employs optimized frequency microstates to decipher the distant cortical communication of visual target detection tasks. The temporal dynamics of the frequency microstate metrics are correlated with fMRI hemodynamic functional connectivity measures to optimize the cortical EEG quasi-stable frequency patterns with the local/global brain communication elicited by the task. The hemodynamic functional connectivity is assessed by employing the graph-theoretical analysis on simultaneously acquired fMRI information. The significantly correlated frequency microstates are further subjected to the robust correlation analysis to understand their multi-frequency coupling elicited during intercortical interaction during the task engagement. The local and global neural mechanisms underlying these frequency quasi-stable microstates were further estimated through EEG-informed-fMRI analysis. Finally, a hybrid deep learning framework consisting of LSTM with attention is employed to classify the target detection task engagement from the temporal dynamics of these optimized frequency microstate quasi-stable patterns. Six deep learning architectures (three LSTM and three attention-based LSTM networks) are trained with all optimized, quasi-stable frequency microstates collected from their associated time segments (200, 300, and 500 ms/segment, respectively) and passed to their respective input cells (15, 10, and 6) of the first LSTM layer. Six deeply layered architectures employed in this study possessed three stacked LSTM layers, and the final LSTM layer was integrated with an attention layer in three attention-based LSTM networks. The performance metrics such as precision, accuracy, and recall are estimated for all six deep learning architectures and validated using a 10-fold cross-validation approach.

2. Methods And Materials

2.1 Participants

Seventy healthy right-handed volunteers (30 males and 40 females; mean age: 23 years; age range, 20–32 years) were selected from the academic environment. All participants gave written informed consent and did not have any psychiatric, or neurological disorders or medication. The experiment was conducted following the World Medical Association (Declaration of Helsinki), and the local ethical committee approved all measurements. The vision of participants was corrected using MR-compatible lenses whenever required.

2.2 Task design

The visual target detection task comprised of a sequence of simple geometrical shapes such as squares, circles, stars, and triangles filled with primary colors were presented, as shown in Fig. 1. The paradigm consisted of 105 sub-trials over five trials, where 32 target stimuli are distributed pseudo-randomly over the sub-trials. Each trial started with the presentation of a 'Target' object for 3 seconds. In subsequent slides, a collection of geometric shapes, one item at a time, is presented for 3 seconds to the volunteer. The volunteer's task was to detect the previously shown target and respond quickly by pressing a button with the right thumb. A single cross in the slide's center is presented for 3 seconds during the fixation period following each task stimulus. All the volunteers are instructed to avoid any motor response during fixation and distractor stimuli. These task stimuli are projected onto MR compatible lenses fitted on the head coil inside MR.

2.3 Simultaneous EEG-fMRI acquisition

In the present study, simultaneous EEG-fMRI data acquisition is carried out using a 3T Siemens Magnetom Skyra scanner (Siemens, Erlangen) and MR compatible 32-channel Brain Amp system with an EEG cap. EEG signals are recorded at a sampling rate of 5 kHz, and the impedance of all scalp electrodes is maintained below five kOhms throughout the recording.

The fMRI were acquired using Eco Planar Imaging (EPI) sequence with TR = 3000 ms; TE = 36 ms; voxel size = 3.6*3.6*3.0 mm; matrix = 64*64; FoV read = 230 mm; flip angle = 90^{o}, 36 axial slices. The axial slices are acquired parallel to the Anterior-Posterior (AC-PC) line in an interleaving manner with a slice thickness of 3.0 mm. The high-resolution structural images of the brain are acquired using T1 MPRAGE sequence with parameters, voxel size = 1.0*1.0*1.0 mm; TR = 2000 ms; flip angle = 90^{o}; FoV = 240 mm; matrix = 512*512; slice thickness = 1.0 mm, 160 axial slices. The axial slices are acquired parallel to the Anterior-Posterior (AC-PC) line in an interleaving manner with a slice thickness of 5.0 mm.

2.4 Data preprocessing

2.4.1 EEG data

The detailed pipeline employed in this study for cleaning both MRI artifacts and other artifacts is the same as our earlier study (Kaur et al. 2020). It employs the FMRIB plugin of EEGLAB that uses combined adaptive thresholding (Christov 2004) and the Teager energy operator (Kim et al. 2004), and the Harvard Automated Processing Pipeline for EEG (HAPPE) (Gabard-Durnam et al. 2018) for noise-free time-

frequency analyses. Then, the data is downsampled to 250 Hz and then re-referenced to the common average reference. Finally, the artifact corrected data of all the participants are then segregated specific to the target, distractor, and fixation blocks.

2.4.2 fMRI data

The fMRI data preprocessing is performed using Statistical Parametric Mapping version 12. The data is corrected for slice-timing differences and spatially realigned and excluded if movement exceeds 3 mm. It follows by registering the functional scans to standard MNI template space. The preprocessed images are subjected to spatially smoothing with 5*5*5 mm full width half maximum Gaussian kernel.

2.5 Data Analysis

The present study develops a computational framework that classifies distinct task engagement's temporal global cortical communication through unique temporal EEG quasi-stable information that decodes the neural basis of the distant cortical communications. Figure 2 explains these processes in detail. The following section will elaborate on each one of these steps in detail.

2.5.1 Estimation of frequency-microstates and their association with task's cortical communications

At first, artifact-corrected EEG data is band-pass filtered to segregate it into frequency-band limited data comprising of (1–4) Hz for delta, (4–8) Hz for theta, (9–14) Hz for an alpha, (15–35) Hz for beta and (35–48) Hz for gamma. Then, the Global Field Power (GFP) of each frequency information is computed and subjected to the modified K-means clustering algorithm (Pascual-Marqui et al. 1995) to identify every frequency microstate topographic prototype. A detailed description of this estimation is given in the supplementary file (section S.1). Then, each frequency microstate prototype is back fitted in every individual's data and estimated re-expressed sequences of microstate classes. Finally, statistics about the sequence of microstate classes, such as their frequency of occurrence or average duration, are calculated. This quasi-stable frequency-microstate patterns elicitation information is subsequently mapped with global functional connectivity of each task engagement assessed from simultaneously acquired fMRI information.

Global functional connectivity estimation from simultaneously acquired fMRI information

At first, General Linear Model-based analysis was employed using simultaneously acquired fMRI information to identify the task's neural correlates. At the subject level analysis, BOLD responses of each task engagement (target, distractor, and fixation) are modeled by a canonical hemodynamic response function with temporal and dispersion derivatives with six realignment parameters for each run. In second-level GLM modeling, group average maps were computed using one-sample t-tests, cluster corrected ($p < 0.05$) across subjects. Subsequently, the second-level GLM model results for every task engagement are passed as Regions of Interest (ROI) to graph theory analysis to estimate the global/local functional connectivity (Whitfield-gabrieli and Nieto-castanon 2012). A detailed description of this

estimation is given in the supplementary file (section S.2). Finally, the graph theory metrics such as global and local efficiency of the functionally connected regions are estimated for each subject, and the ROI-to-ROI connectivity matrix is thresholded at p-FDR < 0.05 in a two-sided analysis.

Optimization of frequency-microstate elicitations with fMRI functional connectivity measures and their validation through Microstate informed fMRI

This study examines whether cortical quasi-stable frequency EEG elicitation could be employed to explain temporal global cortical communications of different task engagements. For this purpose, the number of occurrences of each delta, theta, alpha, beta, and gamma EEG-microstates of every individual during task engagement (target, distractor, and fixation) is subjected to the robust correlation with global functional connectivities metrics measured from the simultaneously measured fMRI information.

This study further validated these significantly correlating frequency microstates by subjecting them to the EEG-informed fMRI analysis (Huster et al. 2012; Abreu et al. 2018) and studied their neural mechanisms. Since the frequency microstates that correlate with fMRI functional connectivity metrics are different for target, distractor, and fixation, three separate EEG-informed fMRI models were constructed for every task engagement. A detailed description of this estimation is given in the supplementary file (section S.3).

2.5.2 Classification using attention-based LSTM deep learning model

This study primarily aims to develop a computational framework, attention-based Long Short-Term Memory (LSTM), to classify the glocal cortical communication using frequency quasi-stable oscillations associated with the global brain communications observed in fMRI functional connectivity. LSTM has been a popular recurrent neural network for learning sequential features in time series data and classifying EEG information (Wang et al. 2018; Nagabushanam et al. 2020). The attention mechanisms have been recently conceptualized (Vaswani, A. 2017) and integrated with the LSTM framework and found helpful in classifying the data that involves remembering and aggregating feature embeddings in time-series information (Zhang et al. 2020a). Due to the discrepant and task-dependent nature of the task's EEG information, attention-based LSTM architecture is more suited and employed in our study for classifying the task's EEG signals. Hence, at first, each frequency-microstate strongly associated with fMRI functional connectivity measures was correlated with every individual preprocessed EEG information. Then, the feature vector consisting of the correlation value for each quasi-stable frequency microstates belonging to every task engagement is formed and used as a training, testing, and validation dataset for the attention-based LSTM deep learning model. A detailed description of the deep attentional LSTM Model and the fine-tuning process is given in the supplementary file (section S.4). Figure 3 clearly explains these processes in detail. Table 1 provides the information on the fine-tuning parameter adopted for the deep learning model.

As the sampling rate of the EEG data is 250Hz, 250 feature vectors were compiled for every second, with a single vector covering every 4 ms neural activity. Each task engagement was carried out for 3 seconds; there are 750 feature vectors staggered for every task block. To avoid feeding too many features to the architecture, feature vectors are combined across task blocks, and three distinct segregation of input feature vectors (200ms/segment, 300ms/segment, and 500ms/segment) belong to every task block were explored. The study independently employed three distinct attention-based LSTM architectures in input layers with 15, 10, and 6-LSTM cells. The final LSTM layer of all the three architecture was ensued by an attention layer, succeeded by a fully connected layer having a sigmoid activation function to predict the probability of each task engagement. Finally, to estimate the efficacy of attention mechanisms in the original LSTM system, all the three attention-based LSTM architectures were compared with their attention counterpart.

Table 1
Final Tuning parameter of LSTM model.

Hyperparameters	Tuned parameters
Hidden layer size	256
Batch size	64
Training epoch numbers	1000
Rate dropout	Input Layer: 0, 1st LSTM Layer: 0.2, 2nd LSTM Layer: 0.1, 3rd LSTM Layer: 0.2
Recurrent depth	3
Learning rate	0.001

Validation approach:

Finally, the proposed deep learning architecture is validated by employing a 10-fold cross-validation approach with no overlap of training and testing segments. True Positive (TP), True Negative (TN), False Negative (FN), and False Positive (FP) were used to calculate the performance metrics. They are formulated as Precision = TP/(TP + FP), Accuracy = (TP + TN)/(TP + TN + FP + FN) and Recall = TP/(TP + FN).

3. Results

The present study presents the times series computational frameworks that classify different task engagement based on temporal modulation of distant brain communications through optimized frequency EEG microstates. The frequency EEG microstates were optimized by associating them with simultaneously eliciting distant hemodynamic functional connectivity measures. Further, the study explored the EEG-informed fMRI approach that has been employed to understand the insights into the

neuronal mechanisms associated with frequency microstates that correlate with global task communications. The following sections present the results of each of the above steps in detail.

3.1 Frontal, parietal, and temporal cortical interaction elicited during different task engagements:

The neural correlates associated with each task engagement are assessed through GLM models in fMRI information with the double-sided t-test of $p < 0.5$, FDR corrected. The results suggest that target engagement enhanced the hemodynamic response in the frontal (frontal orbital cortex (FOC), frontal pole (FP), superior frontal gyrus (SFG), parietal (angular gyrus (AG), Precuneus cortex (PC)), and temporal (Inferior and middle temporal Gyrus (ITG, MTG)) cortices. Further, it involves significant engagement of the cingulate gyrus (CG), lateral occipital cortex, occipital pole (OP), paracingulate gyrus, and insular cortex (IC) regions. The neural correlates of distractor and fixation have also revealed distinct intercortical engagement. The detailed list of neural correlates of each task engagement is tabulated in Supplementary Table (ST.1).

The presence of this distinct inter cortical communication during each task engagements are furthur supported by the graph theoritical functional connectivity metrics such as global (GE) and local efficiency (LE). The target engagement significantly engaged inter and intra-cortical communication at frontal cortex (frontal pole [GE:0.893, LE:0.89], frontal orbital cortex [GE: 0.886, LE:0.89], and superior frontal gyrus [GE:0.886, LE:0.894]), parietal cortex (left angular gyrus [GE:0.872, LE:0.893], right angular gyrus [GE:0.9, LE:0.887], precuneus cortex [GE:0.87, LE:0.894]) and temporal cortical regions (inferior temporal gyrus [GE: 0.88, LE: 0.889], middle temporal gyrus [GE:0.889, LE: 0.891], temporal occipital fusiform cortex [GE:0.88, LE:0.89]) at $p < 0.05$ with FDR correction.

Functional connectivity elicitation remained distinct during this target detection task and had minimal overlap in neural mechanisms, regions, and intracortical interaction with each task engagement. Notably, frontoparietal and frontotemporal interaction engagement was distinct at the neuronal level for target, distractor and fixation engagement. The detailed information of graph-theoretical measures estimated for each task engagement is given in the supplementary file (section S.2).

3.2 Quasi-stable frequency-microstates and their association with task's fMRI functional connectivity measures

As mentioned in the data analysis section, the preprocessed band passed EEG information of every task engagement (target, distractor, fixation) is subjected to the frequency-microstate estimation. Four dominant frequency microstates are estimated for every EEG frequency band of each task engagement. Figure 4 illustrates spatial topographical patterns of each frequency-microstate topography associated with every task engagement.

Further, the number of occurrences of every task's frequency-microstate prototype is estimated by back-fitting these frequency-microstates to every volunteer's respective frequency information. Figure 5 compares the mean number of occurrences of all volunteers of each frequency-microstate across every task. Most of the researchers in the literature use the alphabetical approach to label each microstate. This nomenclature brings difficulty in following similar observations across the literature. Hence, in this study, the unique directional pattern of each microstate's moderate activation band (green colour band) is used for labelling these microstates. In this study, based on the microstate's green colour band direction, they are labelled as anterior-posterior (AP), left-right (LR), left diagonal (LD), and right diagonal (RD) microstate prototypes. For example, the delta microstate with a green band travelling between anterior-posterior is called the "anterior-posterior delta microstate". As the study primarily focuses on identifying the frequency-microstate that manifests the cortical communication elicits during the task engagement, every frequency microstate's number of occurrences is robustly correlated with the fMRI functional connectivity measures. The significantly ($p < 0.01$) correlating frequency microstates were colour-coded (+ ve correlation: green, -ve correlation: red) in Fig. 5.

The significantly associated, optimized frequency microstates with graph-theoretical measures of every task engagement are illustrated in Fig. 6. A total of twelve frequency microstates (target: 4, distractor: 4 and fixation: 4) significantly correlated with the functional connectivity measures of simultaneously acquired fMRI information. During target engagement, the number of occurrences of right diagonal delta-microstate positively correlates with the global efficiency of fMRI functional connectivity measures. On the other hand, the local efficiency of fMRI connectivity measures correlates negatively with both left-right theta and alpha microstate occurrences and positively with anterior-posterior theta microstate.

3.3 Neurovascular analysis of optimized frequency microstates: EEG Informed fMRI analysis

Engagement of task generally elicits local neural clustering (high-frequency quasi-stable oscillations) at distinct brain regions, responsible for efficient local information processing, together with distant cortical intercommunication to facilitate global communication (low-frequency quasi-stable oscillations). The neuro-vascular analysis through EEG-informed fMRI explains these insights through synchronizing neural information (optimized quasi-stable EEG oscillations) with hemodynamic information (vascular) that is elicitated from a specific task engagement. For this purpose, each one of twelve optimized frequency microstates is processed in independent EEG-informed fMRI models, which modelled each microstate as independent regressors ($p < 0.01$, FDR corrected) to estimate their neuro-vascular information. Supplementary figures (SF.1(a-c)) show neuro-vascular information of each twelve optimized microstates.

Figure 7 shows the neuro-vascular coupling of each significant frequency-microstate at the neural correlates of the respective task engagement. The figure also shows the functional connectivity between each neural correlate of task engagement. It is further evident from Fig. 7 that fMRI functional connectivity optimized frequency microstate associates with almost most of the brain regions involved in

each task engagement. Target engagement elucidated the right-diagonal delta-microstate synchronously with the BOLD response in the frontal cortex. Further, anterior-posterior and left-right theta-microstates are found to synchronize with the BOLD response of frontal, temporal, parietal, and occipital regions except for right-lateralized SFG and AG. The role of theta-microstate in BOLD-synchronization of these regions characterizes its significant association with target engagement. The alpha-microstate is observed de-synchronizing with the parietal, PCG's BOLD response, and synchronizing with the frontal, occipital region during target engagement. Our findings also reveal the effects of multiple frequencies on specific brain regions, such that the BOLD response of FP, PCG, SFG, IC, PC, and AG are modulated with delta, theta, and alpha-microstates. Specifically, the study observes the de-synchronization of alpha-microstate with the delta and theta microstates such as PCG, SFG, PC, and synchronization between delta and theta microstates as IC and FP. Hence, the relationships mentioned above reveal that the multi-frequency interactions modulate the BOLD response of task-engaged brain regions.

Performance of Deep Attentional LSTM Model:

The performance of the proposed deep attentional model revealed that hybrid deep learning architecture allows it to apply the attention layer that finds meaningful patterns using LSTM by overcoming the fixed-length input sequences. Figure 8 compares the performance metrics, precision, accuracy, and recall of all the six deep learning models (LSTM and attention-LSTM) in classifying the different task engagement based on the stacked feature vectors that consist of correlation information of each optimized frequency microstate. Three distinct segregation of input feature vectors (200ms/segment, 300ms/segment, and 500ms/segment) with 15, 10, and 6-LSTM cells in input layers were analyzed within the context of each type of network (LSTM and attention-LSTM). As can be observed, LSTM combined with attention appears to perform significantly better in three of the performance metrics. In this case, the choice of nodes (15, 10, and 6) that depends on the EEG time series window (200ms, 300ms, and 500 ms) seems reasonable since it reflects a significant variation in the precision, accuracy, and recall. The results reflected improved performance for using ten nodes from six nodes; a significant decline in performance metrics is observed for using 15 nodes from 10 nodes. In this regard, the proposed attention-based LSTM architecture has proven to enhance the model performance. However, the choice of nodes for the first layer of LSTM architecture leads to variation in deep learning architecture performance.

4. Discussion

The present study brings more insights into understanding and optimizing frequency microstate information estimated from cortical, coarse EEG information with distant fMRI functional connectivity measures associated with different task engagements and then utilizes them to train a times series of deep learning frameworks. The study employs an attention-based stacked LSTM for effectively remembering and aggregating feature embeddings in the time-series classification of stacked temporal dynamics of the frequency microstate quasi-stable patterns. The results reveal that combining quasi-stable frequency microstates (optimized by the functional connectivity) with an attention-based LSTM algorithm better classifies target engagement, distractors and fixation. Further, the study has also

employed EEG informed fMRI to understand the optimized frequency microstates' neuro-vascular insights and mechanisms. The following section discusses those observations in detail.

4.1 Association of distinct frequency microstates with each task's cortical functional connectivities

The study observed four distinct cortical frequency-microstates elicitations for each of three different task engagements (thus, twelve distinct frequency microstates) correlated strongly with their hemodynamic functional connectivity measures independently. Nonoverlap of association of these frequency microstates clearly states the underlying difference in distant cortical communications associated with each task engagement. In addition, the study also has observed a distinct neuro-vascular functional association of slow and faster oscillations in the brain regions involved in each task's cortical communications. Some of the essential observations related to these multi-frequency quasi-stable EEG frequency associations with each task's distant neural interactions are summarized below.

Elicitations of slower and faster quasi-stable microstates oscillations and their sync/desynchronization with task's global/local neural engagements:

Complex cognitive engagement requires global interactions of different brain regions enabling the large-scale integration of local neural information. The integration of neural engagement of spatially distant regions constituting the large-scale networks is primarily moulded with low-frequency synchronized oscillations due to their long-range communications and integrative roles in various brain functions.

Further, the strength of large-scale networks has also been found highest for lower frequencies and seen gradually decreasing with increases in the frequency range (Wu et al. 2008; Gohel and Biswal 2015; Li et al. 2015). Therefore, the dominance of large-scale networks for the lower range of frequencies confirms their functional significance. The present study's results (Fig. 6) distinctly revealed synchronization (positive correlation) of the slow frequency oscillations with global, distant brain communication and desynchronized (negative correlation) with local neural elicitation across all the task engagement. Similarly, the high-frequency quasi-stable oscillation distinctly synchronized with the elicitation of local neural engagement and desynchronized with global communications across all the task engagements. A similar observation (Fig. 7) is revealed in the neurovascular coupling from EEG-informed fMRI analysis at the brain regions engaged in all tasks. They demonstrated significant desynchronization between slow and faster quasi-stable oscillations in most brain regions involved during every task engagement. Further, the region-wise neuro-vascular insights brought slower quasi-stable oscillations associations with large-scale frontoparietal and frontotemporal functional networks. These observations are supported by the proposal of Polich et al (Polich 2007) and Harper et al, (Harper et al. 2017) explaining the role of delta and theta band activity underlying the frontoparietal and frontotemporal functional networks.

The accumulating literature suggests the association of local neuronal processing with the global cortical communication between neural assemblies by coupling multiple oscillatory frequencies (Canolty and

Knight 2010) and referred to as cross-frequency coupling. The most well-studied example of cross-frequency coupling is the theta-gamma coupling, which explains the engagement of gamma frequency in certain phases of theta cycles. Further, (Schroeder and Lakatos 2009) suggested that low-frequency oscillations may provide an essential role in engaging gamma rhythms during attention. (Lisman and Jensen 2013) discussed the relationship of alpha and theta frequency oscillations in the cortex and revealed the possibility of the theta-gamma code's contribution to memory and sensory processes. Thus, the functional interaction of more extensive networks oscillating at lower frequencies and local neuronal ensembles oscillating at higher frequencies has been revealed for cortical communication and integration (Fell and Axmacher 2011; Lisman and Jensen 2013; Knyazev et al. 2019). Hence, the studies mentioned above better understand the modulation of faster oscillations from the slow EEG oscillations during cognitive engagements.

The present study's quasi-stable cortical oscillation's neuro-vascular insights and their association with local and global neural information are consistent with these studies and explain the role of multi-frequency interactions in explaining the complex cognitive engagements' neuronal mechanisms.

4.2 Performance of attention-based deep learning system in classifying time series quasi-stable cortical frequency EEG information

All six proposed deep learning architectures demonstrated in Fig. 3 revealed comparable accuracy, precision, and recall rate for classifying target detection task engagements. However, two primary aspects distinguished the performance of each proposed deep learning architecture. They are the temporal sampling window and incorporation of the attention mechanism.

4.2.1 Temporal sampling window of quasi-stable frequency information optimizes the performance of deep learning architectures

Temporal sampling window size plays a significant role in achieving the best classification accuracy of deep learning architectures. This crucial aspect of time-locked microstates events facilitated a better temporal data handling of multi-frequency interaction in the cognitive task's neural engagements. The present study employed three different windows of temporal sampling (six nodes: 500ms, ten nodes: 300 ms, and fifteen nodes: 200 ms) to explore optimized, quasi-stable microstate's ability to classify task engagement. The highest classification accuracy, up to a 96% accuracy for ten node attention-based architecture, confirms the temporal dynamics of quasi-stable frequency oscillations optimally with 300ms. Several target identification-related EEG studies support this observation (Bledowski et al. 2004; Bansal et al. 2014; Sclocco et al. 2014; Pandey et al. 2016; Arvaneh et al. 2019) revealed that the peak of task event-related potentials following the stimulus onset in between 100 ms to 300 ms at multiple.

Specifically, a recent EEG study (Harper et al. 2017) showed event-related synchronization of theta and delta bands occurring around 300 ms after the onset of target stimuli.

4.2.2 Effect of attention mechanism with traditional LSTM architectures

The overall better performance of all the deep learning architectures justified the optimization of quasi-stable frequency-microstate information. However, the attention mechanisms further improved this in the deep learning system. The combined effect of attention phenomena and the LSTM architecture allowed the deep learning architecture to dynamically emphasize the task-relevant neural information in the time series sequence of EEG data and give less attention to other irrelevant information. The improvement in the performance of the attention-based LSTM system can be seen precisely in Fig. 8. The plots suggest that the attention mechanism is optimum for extracting the most relevant task neural features and improves the LSTM's performance compared to independent LSTM.

5. Significance Of The Study

There is extensive literature (Supplementary Table (ST.2)) on employing a deep learning approach to decode task engagement using EEG elicitations. However, most of those works are restricted to the sensory-motor tasks (hand, leg movements, imagery tasks) whose engagement can be localized in a few cortical regions. However, minimal research is engaged to decode the cognitive task engagement's functional connectivity of distant and distinct cortical engagement using the deep learning framework. Further, despite many research studies that microstates are a promising neural signature, their association with the neural mechanisms of task engagement is still not clearly understood (Stam 2005; Tognoli and Kelso 2009; Kim et al. 2021). In addition, not many works in the literature explain the quasi-stable nature of the different EEG frequency oscillations either. The present work employs attention-based LSTM architecture to decode the temporal dynamics of cognitive task engagement through fMRI functional connectivity optimized frequency microstates. Recently, (Sikka et al. 2020) investigated the temporal dynamics of traditional microstates using recurrent neural networks. However, their work did not address the quasi-stable frequency microstate's neural mechanism and modulation during task engagement. Our present work further brings more insights into the attention mechanism's ability to improvise the classification of cognitive task engagement based on the optimized neural signatures. To our current knowledge, the present study is one of the few works that employs simultaneous EEG-fMRI information to optimize the neural signatures for improvising the performance of deep learning architectures.

6. Conclusions

The present study proposes an attention-based deep learning framework that processes temporal dynamics of the twelve distinct, fMRI functional connectivity optimized, quasi-stable frequency microstates to classify different cognitive task engagement. It further utilizes neurovascular insights of

these optimized frequency microstates through EEG-informed fMRI analysis to understand the local and distant cortical interaction revealed by the optimized frequency microstate. This optimized neural information was passed as input information at three distinct temporal samplings windows (200, 300, and 500 ms/segment) to train and validate the attention-based LSTM architecture. The results suggest that the classification accuracies of the attention-based LSTM architectures were better than the traditional LSTM architectures due to the ability of the attention mechanisms in deep learning systems in localizing temporal feature information. Notably, the attention-based LSTM model with 300 ms temporal sampling revealed a higher classification accuracy than other architectures. Hence, the study demonstrates an attention-based deep learning framework to perform a robust classification of complex, distant cortical engagement and communication caused by cognitive task engagements based on the novel, quasi-stable frequency microstates.

Declarations

Availability of data and materials: The datasets used and/or analysed during the current study are available from the corresponding author on reasonable request.

Competing interests: The authors declare that they have no competing interests.

Funding: This research did not receive any specific grant from funding agencies in the public, commercial, or not-for-profit sectors.

Authors' contributions: The study was designed by SA and VC. Data was acquired and processed by SA. Data was interpreted and analyzed by VC, SA, and RS. The manuscript was written by SA with the help of VC. All authors reviewed the manuscript.

Acknowledgments: Not applicable.

References

1. Abreu R, Leal A, Figueiredo P (2018) EEG-informed fMRI: A review of data analysis methods. Front Hum Neurosci 12:1–23. https://doi.org/10.3389/fnhum.2018.00029
2. Ahmadi N, Pei Y, Carrette E, et al (2020) EEG-based classification of epilepsy and PNES: EEG microstate and functional brain network features. Brain Informatics 7:. https://doi.org/10.1186/s40708-020-00107-z
3. Akam T, Kullmann DM (2014) Oscillatory multiplexing of population codes for selective communication in the mammalian brain. Nat Rev Neurosci 15:111–122. https://doi.org/10.1038/nrn3668
4. Arvaneh M, Robertson IH, Ward TE (2019) A P300-Based Brain-Computer Interface for Improving Attention. Front Hum Neurosci 12:. https://doi.org/10.3389/fnhum.2018.00524

5. Bansal AK, Madhavan R, Agam Y, et al (2014) Neural dynamics underlying target detection in the human brain. J Neurosci 34:3042–3055. https://doi.org/10.1523/JNEUROSCI.3781-13.2014
6. Bledowski C, Prvulovic D, Hoechstetter K, et al (2004) Localizing P300 generators in visual target and distractor processing: A combined event-related potential and functional magnetic resonance imaging study. In: Journal of Neuroscience
7. Buzsáki G (2009) Rhythms of the Brain
8. Canolty RT, Knight RT (2010) The functional role of cross-frequency coupling. Trends Cogn Sci 14:506–515. https://doi.org/10.1016/j.tics.2010.09.001
9. Christov II (2004) Real time electrocardiogram QRS detection using combined adaptive threshold. Biomed Eng Online 3:1–9. https://doi.org/10.1186/1475-925X-3-28
10. Croce P, Quercia A, Costa S, Zappasodi F (2020) EEG microstates associated with intra- and inter-subject alpha variability. Sci Rep 10:1–11. https://doi.org/10.1038/s41598-020-58787-w
11. Fell J, Axmacher N (2011) The role of phase synchronization in memory processes. Nat Rev Neurosci 12:105–118. https://doi.org/10.1038/nrn2979
12. Gabard-Durnam LJ, Leal ASM, Wilkinson CL, Levin AR (2018) The harvard automated processing pipeline for electroencephalography (HAPPE): Standardized processing software for developmental and high-artifact data. Front Neurosci 12:1–24. https://doi.org/10.3389/fnins.2018.00097
13. Gohel SR, Biswal BB (2015) Functional integration between brain regions at rest occurs in multiple-frequency bands. Brain Connect 5:23–34. https://doi.org/10.1089/brain.2013.0210
14. Gschwind M, Hardmeier M, Van De Ville D, et al (2016) Fluctuations of spontaneous EEG topographies predict disease state in relapsing-remitting multiple sclerosis. NeuroImage Clin 12:466–477. https://doi.org/10.1016/j.nicl.2016.08.008
15. Harper J, Malone SM, Iacono WG (2017) Theta- and delta-band EEG network dynamics during a novelty oddball task. Psychophysiology 54:. https://doi.org/10.1111/psyp.12906
16. Hipp JF, Engel AK, Siegel M (2011) Oscillatory synchronization in large-scale cortical networks predicts perception. Neuron 69:387–396. https://doi.org/10.1016/j.neuron.2010.12.027
17. Huster RJ, Debener S, Eichele T, Herrmann CS (2012) Methods for simultaneous EEG-fMRI: An introductory review. J Neurosci 32:6053–6060. https://doi.org/10.1523/JNEUROSCI.0447-12.2012
18. Jiang M, Gu J, Li Y, et al (2021) HADLN: Hybrid Attention-Based Deep Learning Network for Automated Arrhythmia Classification. Front Physiol 12:. https://doi.org/10.3389/fphys.2021.683025
19. Jin Y, Wu D, Guo W (2020) Attention-based LSTM with filter mechanism for entity relation classification. Symmetry (Basel) 12:1–16. https://doi.org/10.3390/sym12101729
20. Karim F, Majumdar S, Darabi H, Harford S (2019) Multivariate LSTM-FCNs for time series classification. Neural Networks 116:237–245. https://doi.org/10.1016/j.neunet.2019.04.014
21. Kaur A, Chinnadurai V, Chaujar R (2020) Microstates-based resting frontal alpha asymmetry approach for understanding affect and approach/withdrawal behavior. Sci Rep 10:1–25. https://doi.org/10.1038/s41598-020-61119-7

22. Khanna A, Pascual-Leone A, Michel CM, Farzan F (2015) Microstates in resting-state EEG: Current status and future directions. Neurosci Biobehav Rev 49:105–113. https://doi.org/10.1016/j.neubiorev.2014.12.010
23. Kiehl KA, Liddle PF (2003) Reproducibility of the hemodynamic response to auditory oddball stimuli: A six-week test-retest study. Hum Brain Mapp 18:42–52. https://doi.org/10.1002/hbm.10074
24. Kim K, Duc NT, Choi M, Lee B (2021) EEG microstate features according to performance on a mental arithmetic task. Sci Rep 11:1–14. https://doi.org/10.1038/s41598-020-79423-7
25. Kim KH, Yoon HW, Park HW (2004) Improved ballistocardiac artifact removal from the electroencephalogram recorded in fMRI. J Neurosci Methods 135:193–203. https://doi.org/10.1016/j.jneumeth.2003.12.016
26. Kim Y, Choi A (2020) Eeg-based emotion classification using long short-term memory network with attention mechanism. Sensors (Switzerland) 20:1–22. https://doi.org/10.3390/s20236727
27. Knyazev GG, Savostyanov AN, Bocharov A V., et al (2019) Cross-frequency coupling in developmental perspective. Front Hum Neurosci 13:1–10. https://doi.org/10.3389/fnhum.2019.00158
28. Koenig T, Prichep L, Lehmann D, et al (2002) Millisecond by millisecond, year by year: Normative EEG microstates and developmental stages. Neuroimage 16:41–48. https://doi.org/10.1006/nimg.2002.1070
29. Laufs H, Kleinschmidt A, Beyerle A, et al (2003) EEG-correlated fMRI of human alpha activity. 19:1463–1476. https://doi.org/10.1016/S1053-8119(03)00286-6
30. Li X, Kehoe EG, McGinnity TM, et al (2015) Modulation of Effective Connectivity in the Default Mode Network at Rest and During a Memory Task. Brain Connect 5:60–67. https://doi.org/10.1089/brain.2014.0249
31. Lisman JE, Jensen O (2013) The Theta-Gamma Neural Code. Neuron 77:1002–1016. https://doi.org/10.1016/j.neuron.2013.03.007
32. Magri C, Schridde U, Murayama Y, et al (2012) The amplitude and timing of the BOLD signal reflects the relationship between local field potential power at different frequencies. J Neurosci 32:1396–1407. https://doi.org/10.1523/JNEUROSCI.3985-11.2012
33. Mantini (2007) Electrophysiological signature of brain resting state networks. Proc Natl Acad Sci U S A 104:13170–13175
34. Michel CM, Koenig T (2018) EEG microstates as a tool for studying the temporal dynamics of whole-brain neuronal networks: A review. Neuroimage 180:577–593. https://doi.org/10.1016/j.neuroimage.2017.11.062
35. Milz P, Faber PL, Lehmann D, et al (2016) The functional significance of EEG microstates-Associations with modalities of thinking. Neuroimage 125:643–656. https://doi.org/10.1016/j.neuroimage.2015.08.023
36. Milz P, Pascual-Marqui RD, Achermann P, et al (2017) The EEG microstate topography is predominantly determined by intracortical sources in the alpha band. Neuroimage 162:353–361. https://doi.org/10.1016/j.neuroimage.2017.08.058

37. Murta T, Chaudhary UJ, Tierney TM, et al (2017) Phase–amplitude coupling and the BOLD signal: A simultaneous intracranial EEG (icEEG) - fMRI study in humans performing a finger-tapping task. Neuroimage 146:438–451. https://doi.org/10.1016/j.neuroimage.2016.08.036
38. Nagabushanam P, Thomas George S, Radha S (2020) EEG signal classification using LSTM and improved neural network algorithms. Soft Comput 24:9981–10003. https://doi.org/10.1007/s00500-019-04515-0
39. Pandey AK, Kamarajan C, Manz N, et al (2016) Delta, theta, and alpha event-related oscillations in alcoholics during Go/NoGo task: Neurocognitive deficits in execution, inhibition, and attention processing. Elsevier B.V.
40. Pang JC, Robinson PA (2018) Neural mechanisms of the EEG alpha-BOLD anticorrelation. Neuroimage 181:461–470. https://doi.org/10.1016/j.neuroimage.2018.07.031
41. Pascual-Marqui RD, Lehmann D, Faber P, et al (2014) The resting microstate networks (RMN): cortical distributions, dynamics, and frequency specific information flow. 1–14
42. Pascual-Marqui RD, Michel CM, Lehmann D (1995) Segmentation of Brain Electrical Activity into Microstates; Model Estimation and Validation. IEEE Trans Biomed Eng 42:658–665. https://doi.org/10.1109/10.391164
43. Polich J (2007) Updating P300: An integrative theory of P3a and P3b. Clin. Neurophysiol. 118
44. Rashid M, Sulaiman N, P. P. Abdul Majeed A, et al (2020) Current Status, Challenges, and Possible Solutions of EEG-Based Brain-Computer Interface: A Comprehensive Review. Front Neurorobot 14:1–35. https://doi.org/10.3389/fnbot.2020.00025
45. Ribary U, Doesburg SM, Ward LM (2017) Unified principles of thalamo-cortical processing: the neural switch. Biomed Eng Lett 7:229–235. https://doi.org/10.1007/s13534-017-0033-4
46. Schroeder CE, Lakatos P (2009) Low-frequency neuronal oscillations as instruments of sensory selection. Trends Neurosci 32:9–18. https://doi.org/10.1016/j.tins.2008.09.012
47. Sclocco R, Tana MG, Visani E, et al (2014) EEG-informed fMRI analysis during a hand grip task: Estimating the relationship between EEG rhythms and the BOLD signal. Front Hum Neurosci 8:1–13. https://doi.org/10.3389/fnhum.2014.00186
48. Sikka A, Jamalabadi H, Krylova M, et al (2020) Investigating the temporal dynamics of electroencephalogram (EEG) microstates using recurrent neural networks. Hum Brain Mapp 41:2334–2346. https://doi.org/10.1002/hbm.24949
49. Stam CJ (2005) Nonlinear dynamical analysis of EEG and MEG: Review of an emerging field. Clin Neurophysiol 116:2266–2301. https://doi.org/10.1016/j.clinph.2005.06.011
50. Tognoli E, Kelso JAS (2009) Brain coordination dynamics: True and false faces of phase synchrony and metastability. Prog Neurobiol 87:31–40. https://doi.org/10.1016/j.pneurobio.2008.09.014
51. Vaswani, A. et al (2017) Attention Is All You Need. IEEE Ind Appl Mag 8:8–15. https://doi.org/10.1109/2943.974352

52. von Wegner F, Bauer S, Rosenow F, et al (2021) EEG microstate periodicity explained by rotating phase patterns of resting-state alpha oscillations. Neuroimage 224:117372. https://doi.org/10.1016/j.neuroimage.2020.117372
53. Wang P, Jiang A, Liu X, et al (2018) LSTM-based EEG classification in motor imagery tasks. IEEE Trans Neural Syst Rehabil Eng 26:2086–2095. https://doi.org/10.1109/TNSRE.2018.2876129
54. Whitfield-gabrieli S, Nieto-castanon A (2012) Conn: A Functional Connectivity Toolbox for Correlated and Anticorrelated Brain Networks. 2:. https://doi.org/10.1089/brain.2012.0073
55. Wu CW, Gu H, Lu H, et al (2008) Frequency specificity of functional connectivity in brain networks. Neuroimage 42:1047–1055. https://doi.org/10.1016/j.neuroimage.2008.05.035
56. Xie Y, Liang R, Liang Z, et al (2019) Speech Emotion Classification Using Attention-Based LSTM. IEEE/ACM Trans Audio Speech Lang Process 27:1675–1685. https://doi.org/10.1109/TASLP.2019.2925934
57. Yan J, Chen S, Deng S (2019) A EEG-based emotion recognition model with rhythm and time characteristics. Brain Informatics 6:. https://doi.org/10.1186/s40708-019-0100-y
58. Yao Q, Wang R, Fan X, et al (2020) Multi-class Arrhythmia detection from 12-lead varied-length ECG using Attention-based Time-Incremental Convolutional Neural Network. Inf Fusion 53:174–182. https://doi.org/10.1016/j.inffus.2019.06.024
59. Yuan H, Zotev V, Phillips R, et al (2012) Spatiotemporal dynamics of the brain at rest - Exploring EEG microstates as electrophysiological signatures of BOLD resting state networks. Neuroimage 60:2062–2072. https://doi.org/10.1016/j.neuroimage.2012.02.031
60. Zhang G, Davoodnia V, Sepas-Moghaddam A, et al (2020a) Classification of Hand Movements from EEG Using a Deep Attention-Based LSTM Network. IEEE Sens J 20:3113–3122. https://doi.org/10.1109/JSEN.2019.2956998
61. Zhang L, Zhu G, Mei L, et al (2018) Attention in convolutional LSTM for gesture recognition. Adv Neural Inf Process Syst 2018-Decem:1953–1962
62. Zhang Z, Ye S, Liao P, et al (2020b) Enhanced Capsule Network for Medical image classification. Proc Annu Int Conf IEEE Eng Med Biol Soc EMBS 2020-July:1544–1547. https://doi.org/10.1109/EMBC44109.2020.9175815
63. Zheng X, Chen W (2021) An Attention-based Bi-LSTM Method for Visual Object Classification via EEG. Biomed Signal Process Control 63:102174. https://doi.org/10.1016/j.bspc.2020.102174

Figures

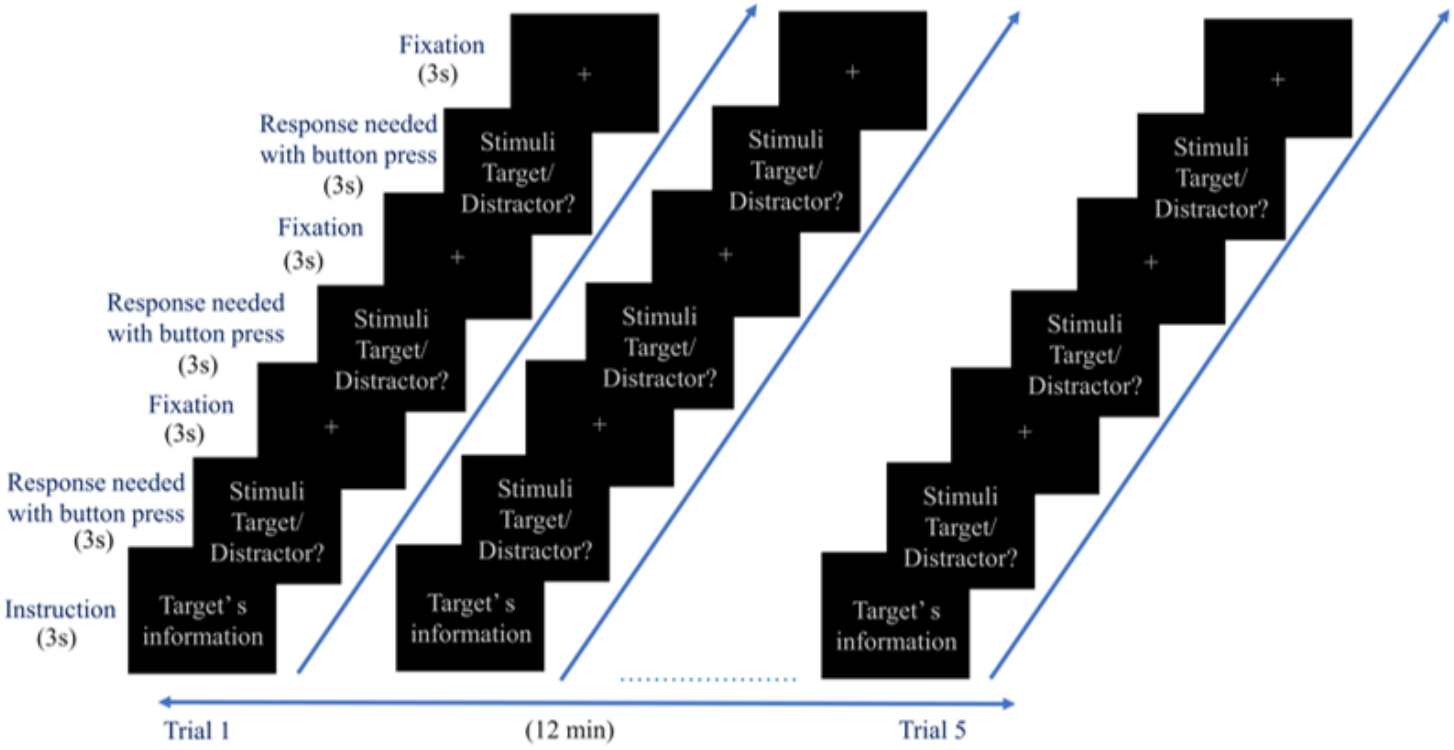

Figure 1

Schematic of visual target detection task design.

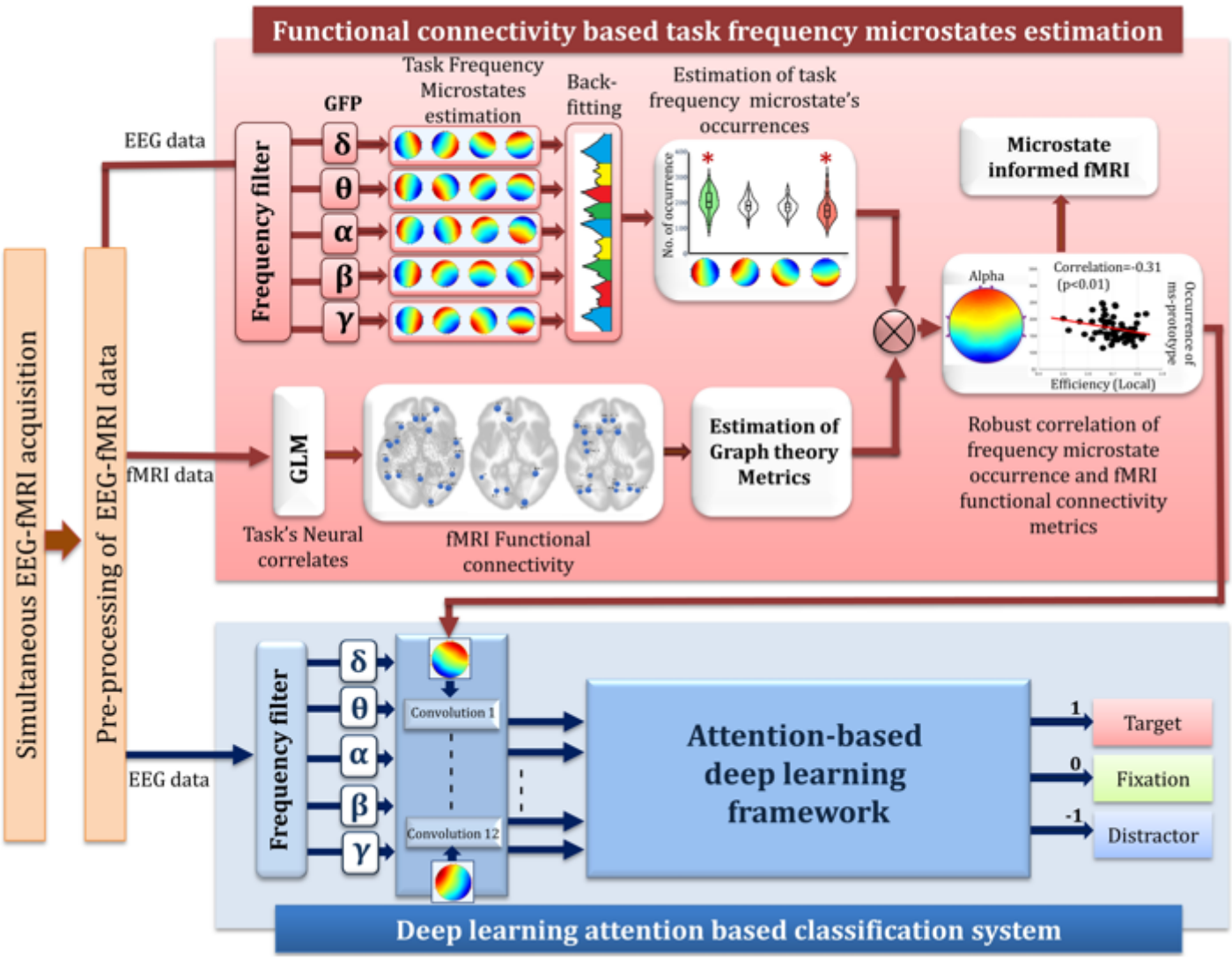

Figure 2

Methodological framework of the study.

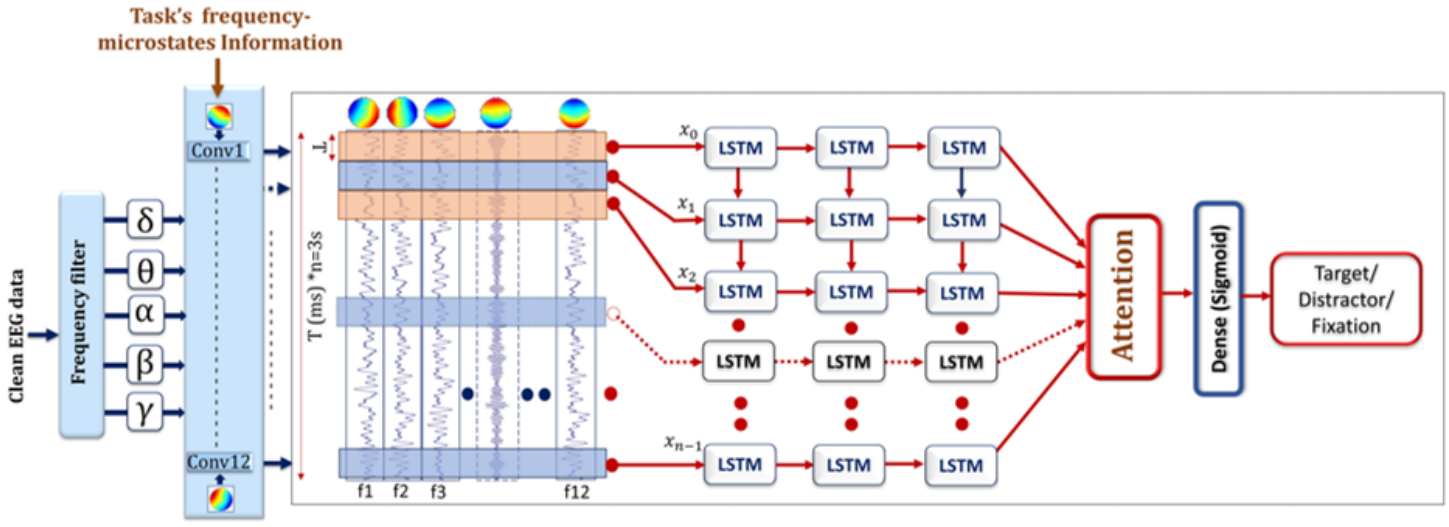

Figure 3

Attention-based LSTM deep learning framework for classification of visual target detection task.

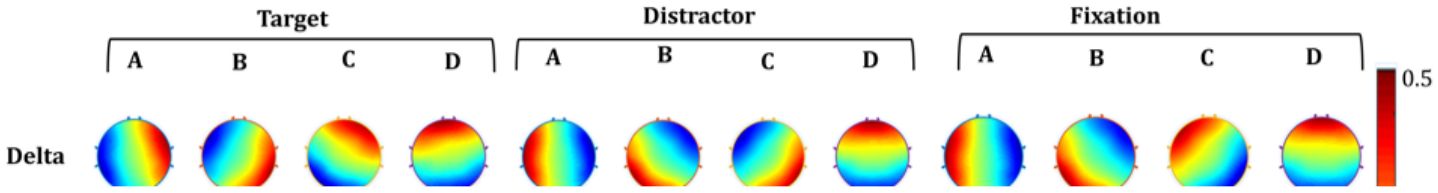

Figure 4

A topographical representation of frequency-microstates for the target, distractor, and fixation.

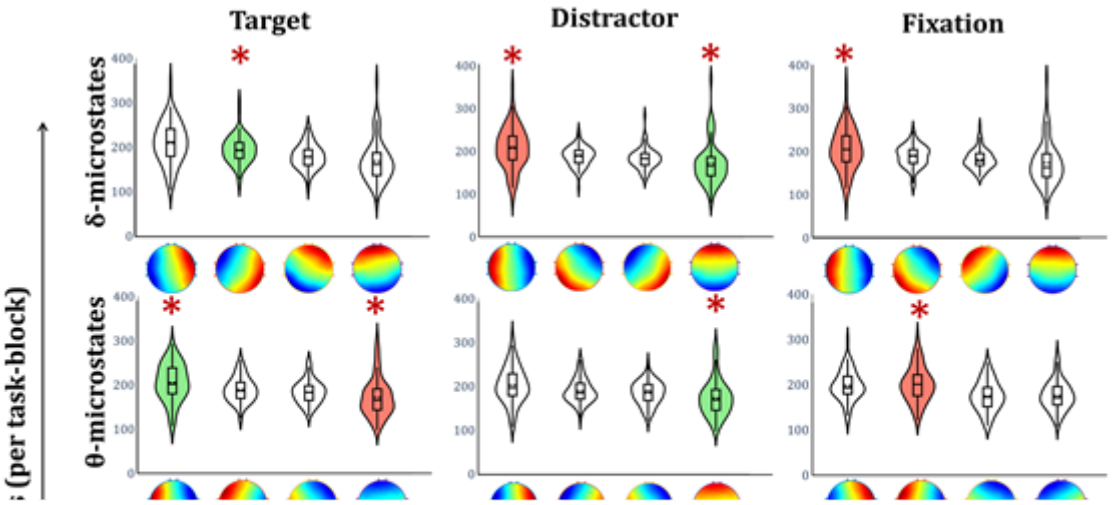

Figure 5

Estimated metrics of frequency-microstates. The violin graph plots the mean occurrence of each frequency-microstates estimated for each frequency band. The violin plot's green and red colour shades reveal the correlation (positive and negative) of the number of occurrences of quasi-stable elicitation with the task's fMRI functional connectivity measures. The red star on violin plots specifies the significance ($p<0.01$).

Figure 6

Significantly associated, optimized, frequency-microstates with graph-theoretical measures of a) Target, b) Distractor, and c) Fixation task engagement. Frequency microstates are labelled as anterior-posterior (AP), left-right (LR), left diagonal (LD), and right diagonal (RD).

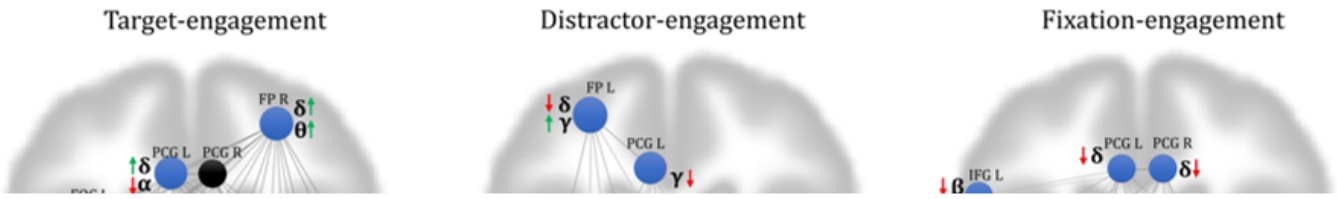

Figure 7

Neuro-vascular coupling of each significant, fMRI functional connectivity optimized frequency-microstates of every task. The Regions shown are neural correlates observed for every task. The neuro-vascular association of optimized frequency microstate with each region is drawn through the arrow next to it (Synchronization: Up green arrow, De-synchronization: Down Red arrow). The region coloured black has no neurovascular association with any one of the optimized frequency microstates.

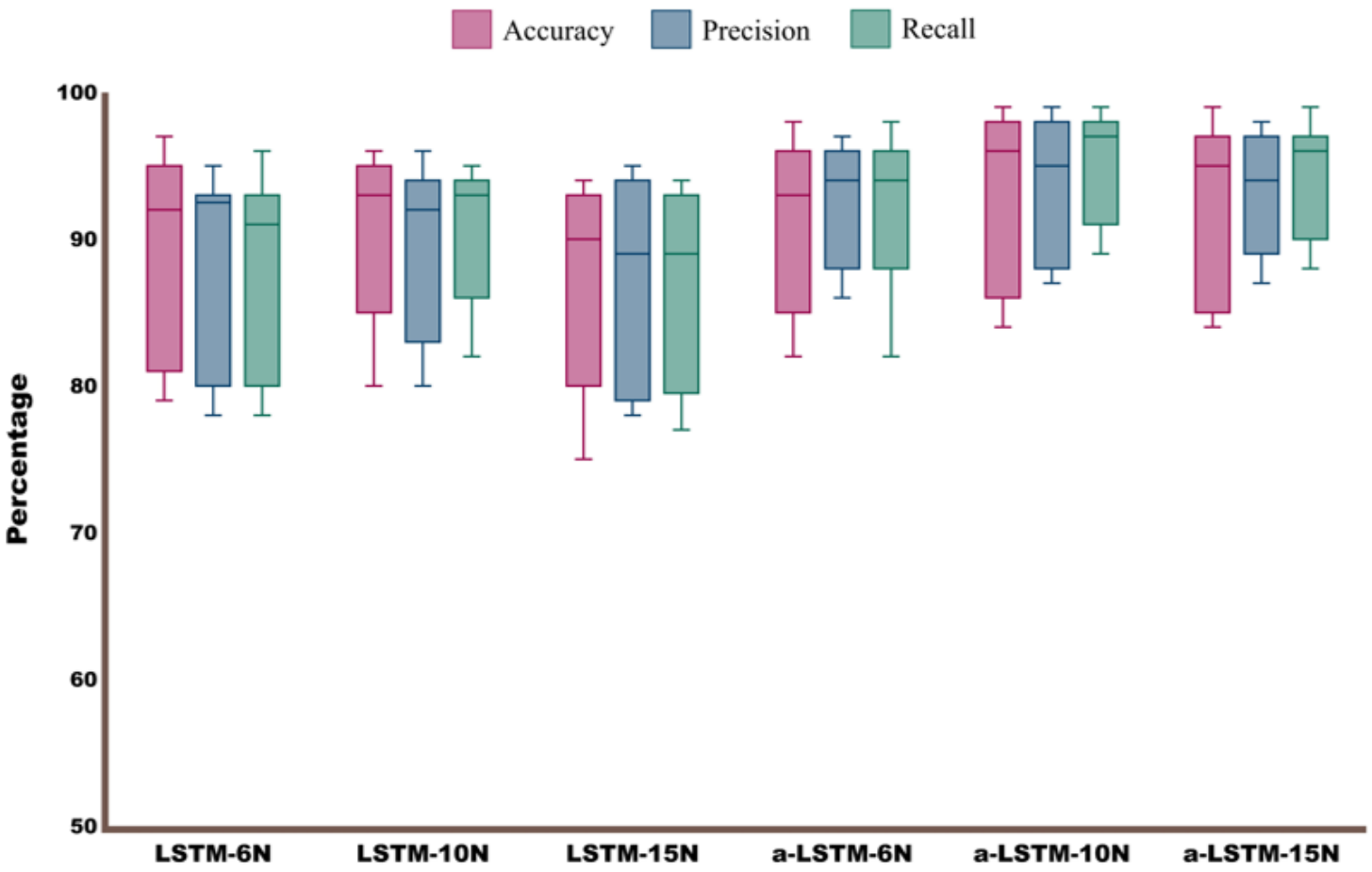

Figure 8

Comparison of performance of the deep learning frameworks between attention-based LSTM and traditional LSTM. The plot reveals the classification performance metrics (accuracy, precision, and recall) for frameworks corresponding to three distinct architectures with 15, 10, and 6-LSTM cells (15N, 10N, 6N) of 200ms/segment, 300ms/segment, and 500ms/segment, respectively.

Supplementary Files

This is a list of supplementary files associated with this preprint. Click to download.

- Supplementaryfile.docx